

Search for Third Generation Scalar Leptoquarks Using the $\tau b \tau b$ Final State

The DØ Collaboration
URL <http://www-d0.fnal.gov>
(Dated: July 20, 2007)

This note describes a search for third generation scalar leptoquarks in $p\bar{p}$ collisions at a center-of-mass energy of $\sqrt{s} = 1.96$ TeV using data with an integrated luminosity of 1.05 fb^{-1} collected by the DØ detector at Run II of the Fermilab Tevatron. This search focuses on the pair-production of third generation scalar leptoquarks (LQ_3) and assumes each leptoquark decays into a τ lepton and a b quark with a branching fraction $\beta = 1$. Therefore, the signature is a di- τ plus di- b -jet final state. One τ is required to decay into a μ and the other τ decays hadronically. No evidence for third generation scalar leptoquark production is observed. Limits are set on $\sigma(p\bar{p} \rightarrow LQ_3 \overline{LQ_3} \rightarrow \tau b \tau b)$ and the third generation scalar leptoquark mass has been excluded at 95% confidence level up to 180 GeV.

Preliminary Results for Summer 2007 Conferences

I. INTRODUCTION

The observed symmetry in the spectrum of elementary particles between leptons and quarks leads to the prediction of the existence of the so-called Leptoquark bosons in many extensions of the Standard Model (SM), *e.g.*, grand unification [1], Technicolor [2] and compositeness [3]. Leptoquarks are either scalar (spin-0) or vector (spin-1) bosons which couple to quarks and leptons via a Yukawa-type coupling, λ , conserving the baryon and lepton numbers. Since flavor-changing neutral currents have not been observed, it is assumed that there are three different generations of leptoquarks, and each couples only to fermions of the same generation. The dominant production mechanism of leptoquarks at the Tevatron, if they exist, is pair production via $q\bar{q}$ annihilation and gluon-gluon fusion.

A leptoquark is expected to decay into a quark and a charged lepton of the same generation with a branching fraction β , or into a quark and a neutrino of the same generation with a branching fraction $(1 - \beta)$. In this note, the results on a search for third generation scalar leptoquarks (LQ_3) that decay with branching fraction β to τb (charge- $\frac{4}{3}$) or to $\tau\bar{b}$ (charge- $\frac{2}{3}$) are presented. For charge- $\frac{4}{3}$ leptoquark, $\beta = 1$. A charge- $\frac{2}{3}$ leptoquark may also couple to $\nu_\tau t$ with a branching fraction $(1 - \beta)$ if it is kinematically allowed. The signature of $p\bar{p} \rightarrow LQ_3\bar{LQ}_3 \rightarrow \tau b\tau b$ process is a pair of highly energetic τ leptons accompanied by two highly energetic hadronic jets which originate from b quarks. Since τ leptons are unstable and soon decay within the detector, it is required that one of the τ leptons further decays into $\mu\bar{\nu}_\mu\nu_\tau$ and the other one decays hadronically in order to achieve better search sensitivity.

Based on the Tevatron Run I data, CDF experiment has set the lowest bound on third generation scalar leptoquark mass at 99 GeV [4] via searches in the $\tau b\tau b$ channel ($\beta = 1$). Run I $D\bar{O}$ and CDF searches in the $\nu\bar{\nu}b\bar{b}$ channel ($\beta = 0$) placed the lowest bounds on charge- $\frac{1}{3}$ third generation scalar leptoquark mass at 94 GeV [5] and 148 GeV [6]. Recently, the $D\bar{O}$ experiment submitted the RunII results of the lowest bounds on the charge- $\frac{1}{3}$ third generation scalar leptoquark mass as 229 GeV for $\beta = 0$ and 221 GeV for the case where $LQ_3 \rightarrow \tau t$ decays occur [7]. CDF also reported their preliminary Run II results on the searches for third generation vector leptoquarks via $\tau b\tau b$ final state and set the cross section limits for LQ_3 pair production at Tevatron [8].

II. DATASET AND MONTE CARLO SAMPLES

The $D\bar{O}$ detector is described elsewhere [9]. This analysis uses data taken by the $D\bar{O}$ detector between April 2002 and February 2006. Events fired by an ‘‘OR’’ of all on-line single muon triggers were selected. The total integrated luminosity is 1.05 fb^{-1} after the good data quality requirement. The efficiency of the ‘‘OR’’ed triggers has been measured and parameterized as a 2D function of muon ϕ and detector η using $Z \rightarrow \mu^+\mu^-$ data and will be applied to the Monte Carlo events.

Six signal Monte Carlo samples of $p\bar{p} \rightarrow LQ_3\bar{LQ}_3 \rightarrow \tau b\tau b$, with different leptoquark masses: 120, 140, 160, 180, 200 and 220 GeV, were generated with PYTHIA [10] version 6.319 where the leading-order (LO) parton distribution function CTEQ6L1 [11] was used. Their cross-sections [12] are calculated at the next-to-leading order (NLO) level.

Most Standard Model processes Monte Carlo samples, such as $t\bar{t}$, W/Z +jets were generated using ALPGEN [13] version 2.05 as a parton level generator, followed by the PYTHIA parton shower and hadronization procedures. The exceptions are the di-boson (WW and WZ) processes which were generated using PYTHIA. For the ALPGEN+PYTHIA samples, a matching scheme (MLM [14]) was included. TAUOLA [15] is used to simulate the tau decay and polarization.

k-factors of 1.39, 1.35 and 1.7 were applied to the $t\bar{t}$, W/Z +light jets and $W/Z + b\bar{b}(c\bar{c})$ samples, respectively, as determined with the MCFM program [16], to account for the NLO cross-sections of these process as compared to the LO cross-sections from ALPGEN. The NLO cross-sections of WZ and ZZ are taken from MCFM [16].

III. OBJECT SELECTION

A. Muon Selection

The muon is selected using hits in the muon detector in combination with track in the central tracking detector, and is required to be within the range of $|\eta_{detector}| < 1.6$, where $\eta_{detector}$ is the pseudorapidity when the center of the $D\bar{O}$ detector is considered as the origin of the coordinate system. The muon is also required to satisfy the isolation requirements in terms of calorimeter energy and tracks momentum around the muon, *i.e.*, the sum of transverse energies of the calorimeter cells, measured with respect to the beam direction, in a halo around the muon direction, $0.1 < R = \sqrt{(\Delta\phi)^2 + (\Delta\eta)^2} < 0.4$, is required to be $\sum_{\text{cells},i} E_T^i < 2.5 \text{ GeV}$; and the sum of the transverse

momenta of all tracks within a cone of $R = 0.5$ around the muon, excluding the muon track itself, is required to be $\sum_{\text{tracks}, i} p_T^i < 2.5$ GeV. Cosmic ray muons are excluded by the cuts on the timing in the Muon scintillators.

B. Tau Selection

Tau decays into hadrons are reconstructed from calorimeter clusters and reconstructed tracks as described in [17]. Taus are separated into three types based on their decay products and the detector responds:

- Type 1: $\tau^\pm \rightarrow \pi^\pm \nu$: a calorimeter cluster with one associated track and no EM sub-cluster;
- Type 2: $\tau^\pm \rightarrow \pi^\pm \pi^0 \nu$: a calorimeter cluster with one associated track and at least one EM sub-cluster;
- Type 3: $\tau^\pm \rightarrow \pi^\pm \pi^\pm \pi^\mp (\pi^0 s) \nu$: a calorimeter cluster with more than one associated track and with or without EM sub-cluster;

For each of the tau types, a neural network [17] is developed to provide the separation of τ lepton and background. The visible τ energy measured by calorimeter alone (E_T) is corrected with the information from the associated tracks for energy and eta ranges where the tracking resolution for charged pions is better than the calorimeter resolution.

A τ candidate is selected if it satisfies the following requirements: (1) the visible corrected transverse energy (p_T) of the τ candidate must be greater than 15 GeV for type 1 or 2 τ candidate, and greater than 20 GeV for type 3 τ candidate; (2) the sum of the transverse momenta of all the tracks associated with the τ candidate (p_T^{trk}) is required to be greater than 5 GeV for type 2 τ candidate, and greater than 15 GeV for type 3 τ candidate. In the case of type 3 τ , at least one of the associated tracks must have $p_T > 7$ GeV; and (3) the τ identification Neural Network output (NN_τ) for a τ candidate should be greater than 0.9 for type 1 or 2 τ , and greater than 0.95 for type 3 τ .

C. Jet Selection

Calorimeter jets are reconstructed from the energy deposited in the calorimeter cells using the Run II cone algorithm with a cone size of $R = 0.5$ [18]. The jet energy has been corrected to the particle level by applying the jet energy scale (JES) [19]. Additionally, jets containing a muon within $\Delta R(\mu, jet) < 0.5$ are corrected for the momentum carried away by the muon and the neutrino, assuming the neutrino carries the same momentum as the muon.

Monte Carlo jets are corrected to take into account the differences between data and Monte Carlo in the jet reconstruction and identification efficiency, the jet energy resolution and the calorimeter responses.

A good jet is required to be with $|\eta_{\text{detector}}| < 2.5$, with $p_T > 20$ GeV and to pass the quality cuts as described in [18].

D. b -jet Tagging

A neural network (NN) based algorithm is used to identify jets originating from b -quarks. Before applying the NN algorithm, jets are required to have at least two associated track. A jet in data is identified as arising from a b -quark if the NN output is larger than 0.2. This corresponds to an efficiency of 72.2% and a misidentification rate of 5.9%. For simulated events, jet flavor dependent identification probabilities are used to determine an overall probability of jet tagging.

E. Missing Transverse Energy

The transverse momenta of undetectable neutrinos can be inferred using momentum conservation in the transverse plane, using the so-called missing transverse energy (\cancel{E}_T) which is the negative sum of the transverse momenta of all particles that were observed in the detector. In practice, the missing transverse energy is calculated by adding vectorially the transverse energies in all calorimeter cells, and then is corrected for the energy calibrations applied to reconstructed jets. \cancel{E}_T is also corrected for the presence of any observed muon.

IV. QCD BACKGROUND

QCD events which pass through the signal selection are required to have $\mu - \tau$ pair with opposite sign (OS). The residual OS QCD events can be described by the same sign (SS) QCD events which are selected using the same signal selections except the $\mu - \tau$ pair having the same sign charges. The number of remaining QCD OS events, N_{QCD}^{OS} , can be estimated by scaling down the number of remaining SS QCD events, N_{QCD}^{SS} , using the following formula:

$$N_{QCD}^{OS} = f(OS/SS) \times N_{QCD}^{SS} \quad (1)$$

in which $f(OS/SS)$ is the scaling factor and the N_{QCD}^{SS} is obtained by subtracting the selected SS MC simulated Standard Model background events (W +jets *etc.*) from the selected SS data events: $N_{QCD}^{SS} = N_{data}^{SS} - \sum_i N_{MC_i}^{SS}$.

$f(OS/SS)$ is derived using a QCD-enriched sample, which is chosen from the same parent dataset by applying the same signal pre-selection requirements (see Sect. V), except requiring there is no isolated μ and no τ candidate fulfilling the criteria in sections III A and III B. Instead, the μ candidate should satisfy the following reversed isolation requirements: $\sum_{\text{cells},i} E_T^i > 2.5$ GeV in $0.1 < R < 0.4$, and $\sum_{\text{tracks},i} p_T^i > 2.5$ GeV in $0.0 < R < 0.5$; and the selected τ candidate is the one with the highest p_T and $NN < 0.9$.

The remaining non-isolated μ data sample is then split into two sub-samples, one with opposite sign (OS) $\mu - \tau$ charges and the other one with the same sign (SS) charge. The scaling factor is the ratio of the excess parts of these two sub-samples over the other MC simulated backgrounds, respectively.

$$f(OS/SS) = \left(\frac{N_{data}^{OS} - \sum_i N_{MC_i}^{OS}}{N_{data}^{SS} - \sum_i N_{MC_i}^{SS}} \right)_{non-iso,\mu} \quad (2)$$

where $(N_{data}^{OS/SS})_{non-iso,\mu}$ is the number of OS/SS non-isolated μ events from data; and $(N_{MC_i}^{OS/SS})_{non-iso,\mu}$ is the number of OS/SS events of each MC simulated SM process with non-isolated μ .

The scaling factors obtained as the function of the p_T of the μ and τ , for samples with different τ type, are shown in Figure 1. For each τ type, the scaling factor is negligibly dependent on the μ or τ p_T , therefore, a constant number is chosen as the scaling factor between the OS and the SS QCD events for each τ type, *i.e.*, $f(OS/SS) = 1.24 \pm 0.09$ for type 1 τ , $f(OS/SS) = 1.09 \pm 0.02$ for type 2 τ events and $f(OS/SS) = 1.03 \pm 0.01$ for type 3 τ events,

The scaling factor is derived after pre-selection and is kept constant for the final optimized selections.

V. PRE-SELECTION AND DATA-MONTE CARLO COMPARISONS

The pre-selection requires the events to pass the following requirements: (1) have only one isolated muon matched with track within the region $\eta < 1.6$ with $p_T > 15$ GeV; (2) the τ candidate should pass the above τ selection requirements, and if two or more pass, the highest p_T candidate is chosen; (3) the τ candidate should have a charge opposite to the muon charge; (4) have at least two good jets which are well separated from the τ candidate by $\Delta R(\tau, jet) > 0.5$, and the p_T of the leading jet should be greater than 25 GeV; (5) have no tight electron as defined in [18] with $p_T > 12$ GeV.

The yields of the data sample and the total numbers of remaining backgrounds after the pre-selection are shown in the second column of Table I. These two numbers are consistent. The expected number of events for each individual Standard Model process as well as the number of signal events (for $m_{LQ_3}=220$ GeV) predicted by the theory at NLO [12] are also shown in this table.

To further verify the Monte Carlo simulation, QCD estimation, object selection, as well as various efficiency corrections to the Monte Carlo samples, comparisons between the data and the Standard Model background expectations for several kinematic and topological variables after pre-selection are performed as shown in Figure 2. The signal process $LQ_3 \overline{LQ_3} \rightarrow \tau b \tau b$ with $m_{LQ_3}=220$ GeV is also shown as reference.

Figure 2 shows the distributions of the p_T of the μ , the τ and the two candidate jets, the distribution of τ identification Neural Network output value for the τ candidates, the type composition of the τ candidates, and the distributions of the event missing transverse energy and the transverse mass calculated from the muon and the missing transverse energy. These plots demonstrate that the data is well described by the Standard Model background expectations at the pre-selection level.

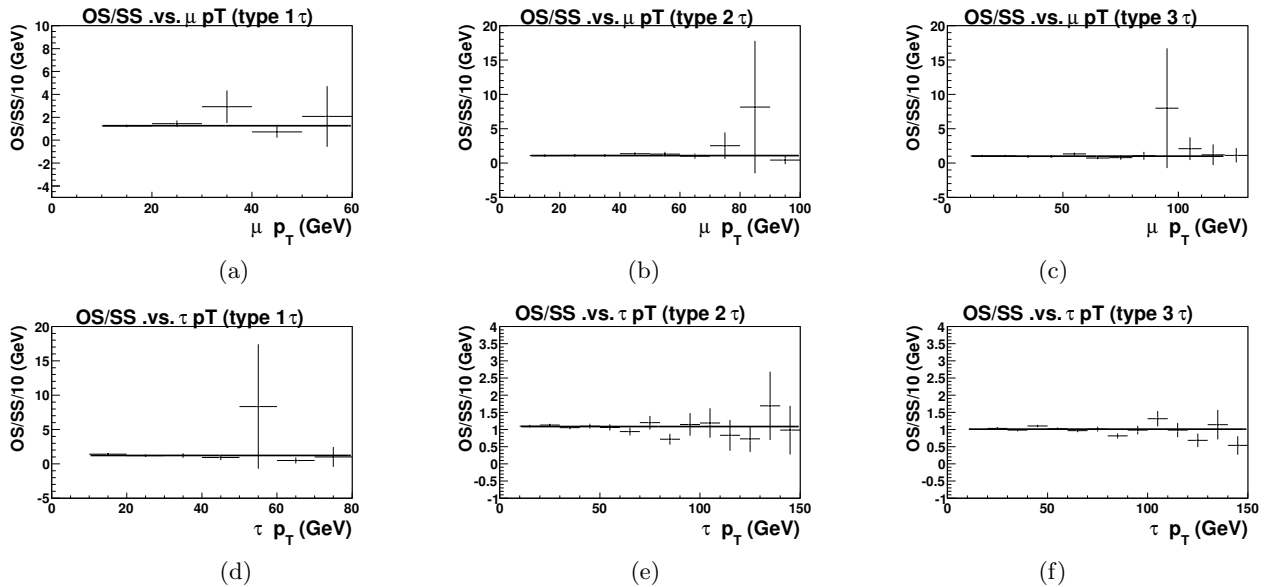


FIG. 1: Distributions of the ratio of the QCD samples with opposite $\mu - \tau$ signs(OS) to the samples with same $\mu - \tau$ signs (SS) as function of μp_T for samples with (a) type I τ , (b) type II τ and (c) type III τ , and as function of τp_T for samples with (d) type I τ , (e) type II τ and (f) type III τ .

VI. FINAL OPTIMIZED SELECTION

After pre-selection, the major contributions to the data sample are expected to be the $Z/W +$ light jets processes, QCD multijets and top pair production, and the expected signal events are still overwhelmed by the background events. To improve the analysis sensitivity, some optimized selections are used to further reduce the background and increase the signal/background ratio.

It is clear from the distribution of the transverse mass calculated from the muon and the missing transverse energy ($m_T(\mu, \cancel{E}_T)$), as displayed in Figure 2 (h), that a large portion of the events from the $W +$ jets and $t\bar{t}$ process are in the W mass region and well separated from the signal, due to the appearance of $W \rightarrow \mu\nu$ in their final states. A cut on $m_T(\mu, \cancel{E}_T) < 50$ GeV is applied. The remaining numbers of data and the expected background are listed in Table I.

To further improve the search sensitivity, the b -jets in the signal are taken into account. Two independent subsamples are selected according to the b -tag of the two selected candidate jets: (1) single-tag sample in which only one of the two candidate jets is b -tagged and (2) double-tags sample in which both two candidate jets are b -tagged. The corresponding numbers of data, of expected backgrounds and of expected signal events for $m_{LQ_3} = 220$ GeV are listed in Table I. Table II shows the signal efficiencies of single-tag and double-tags subsamples for six LQ_3 mass hypotheses.

For each subsample, a so-called S_T variable is constructed as the scalar sum of the p_T of the muon candidate, of the tau candidate, of the two candidate jets and of the event missing transverse energy

$$S_T = p_T(\mu) + p_T(\tau) + p_T(\text{jet1}) + p_T(\text{jet2}) + \cancel{E}_T, \quad (3)$$

which manifests distinct difference between the distributions of leptoquark signal (at high value) and expected backgrounds (at low value) as shown in Figure 3. Instead of making a simple cut, the S_T spectrum will be used as the input final discriminant variable for the limit calculation to achieve better search sensitivity.

As shown in Table I and Figures 2 and 3, at each selection step, the data is well described by the standard model processes, no signal evidence is observed as an excess in data over background. Therefore, the cross section upper limits on the third generation leptoquark pair production will be derived after reviewing the systematic uncertainties.

VII. SYSTEMATIC UNCERTAINTIES

Various sources of systematic uncertainties have been considered in this analysis.

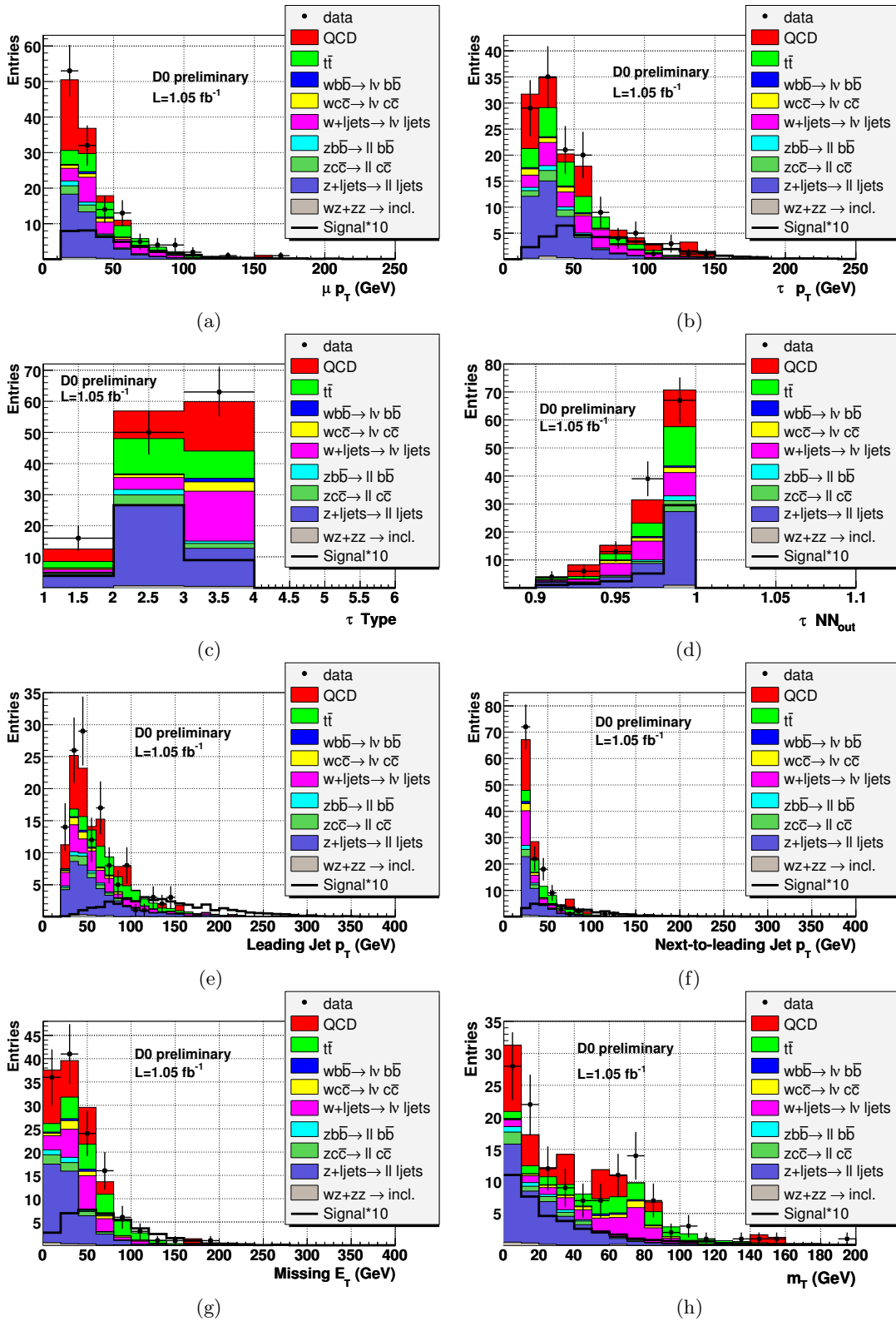


FIG. 2: The distributions of the (a) p_T of μ candidate, (b) p_T of τ candidate, (c) type of τ candidate, (d) τ identification Neural Network output of τ candidate, (e) leading jet p_T , (f) next-to-leading jet p_T , (g) event E_T , and (h) transverse mass calculated from μ and E_T . The signal curve is shown for $m_{LQ_3}=220 \text{ GeV}$.

| Cut | Pre-Selection | $m_T < 50$ GeV | single-tag | double-tags |
|---------------|-------------------|------------------|------------------|-----------------|
| $t\bar{t}$ | 21.94 ± 0.21 | 7.08 ± 0.10 | 3.50 ± 0.06 | 2.11 ± 0.05 |
| Wbb | 1.41 ± 0.12 | 0.46 ± 0.07 | 0.22 ± 0.05 | 0.02 ± 0.01 |
| Wcc | 4.28 ± 0.39 | 1.55 ± 0.24 | 0.42 ± 0.13 | 0.03 ± 0.01 |
| W+lp | 20.64 ± 1.23 | 6.59 ± 0.74 | 0.60 ± 0.22 | 0.02 ± 0.01 |
| Zbb | 2.79 ± 0.09 | 2.39 ± 0.09 | 1.19 ± 0.06 | 0.27 ± 0.03 |
| Zcc | 5.28 ± 0.38 | 4.62 ± 0.38 | 1.14 ± 0.11 | 0.09 ± 0.05 |
| Z+lp | 42.18 ± 0.58 | 37.75 ± 0.60 | 3.48 ± 0.17 | 0.09 ± 0.03 |
| di-B | 1.41 ± 0.14 | 1.15 ± 0.13 | 0.25 ± 0.06 | 0.04 ± 0.02 |
| QCD | 31.31 ± 1.49 | 19.90 ± 1.07 | 3.99 ± 0.34 | 0.89 ± 0.08 |
| total BKGD | 131.25 ± 2.11 | 81.50 ± 1.52 | 14.79 ± 0.51 | 3.56 ± 0.11 |
| Data | 129 | 78 | 16 | 1 |
| Sig.(220 GeV) | 3.80 ± 0.09 | 2.93 ± 0.07 | 1.37 ± 0.04 | 1.08 ± 0.04 |

TABLE I: The number of data, of expected background events (of the sum of all backgrounds as well as of each individual source) and of expected signal events for $m_{LQ_3}=220$ GeV, after successive selections of pre-selection, transverse mass of μ candidate and missing transverse energy, and of single-tag and double-tags subsamples. The uncertainties are statistical only.

| $m(LQ_3)$ (GeV) | Signal Efficiency ($\epsilon(\%)$) | | |
|-----------------|--------------------------------------|-----------------|-----------------|
| | $m_T < 50$ GeV | single-tag | double-tags |
| 120 | 1.13 ± 0.04 | 0.54 ± 0.03 | 0.36 ± 0.02 |
| 140 | 1.43 ± 0.04 | 0.67 ± 0.03 | 0.47 ± 0.03 |
| 160 | 1.59 ± 0.05 | 0.74 ± 0.03 | 0.55 ± 0.03 |
| 180 | 1.71 ± 0.05 | 0.81 ± 0.03 | 0.60 ± 0.03 |
| 200 | 1.78 ± 0.05 | 0.83 ± 0.04 | 0.64 ± 0.03 |
| 220 | 2.01 ± 0.05 | 0.94 ± 0.04 | 0.74 ± 0.03 |

TABLE II: Signal efficiencies of single-tag and double-tags subsamples for six LQ_3 mass hypotheses. The uncertainties are statistical only.

The uncertainty on the efficiencies of μ identification, track match and isolation is determined to be 5% and the efficiency of μ trigger has a 3% uncertainty. The uncertainty on the tau reconstruction efficiency and the tau identification Neural Network output is taken to be 4% and the tau energy correction uncertainty is 2%. The uncertainty on the jet reconstruction and jet identification efficiency is 3% and the uncertainty on jet energy scale (JES) is estimated to be 9% for heavy flavor jets, and 6% for light jets. The uncertainty on QCD estimation is assigned to be 12% by varying the μ isolation cuts from 2.5 GeV to 4 GeV. The b-tagging uncertainty is estimated

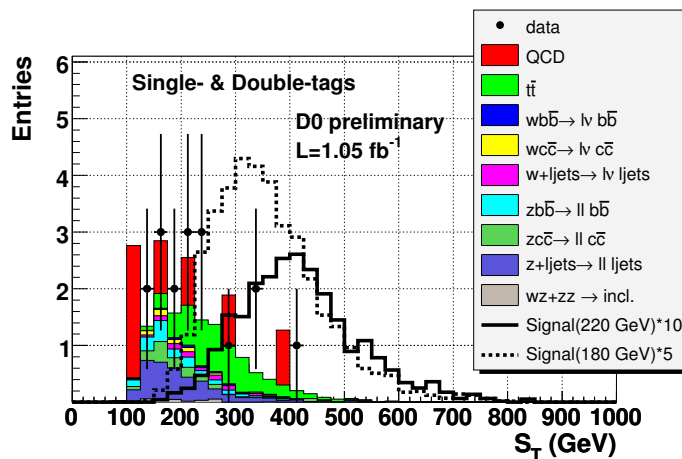


FIG. 3: The S_T distribution for the combination of the single-tag subsample and double-tags subsample. The signal curves are shown for $m_{LQ_3}=180$ GeV and $m_{LQ_3}=220$ GeV.

to be 7.5% for heavy flavor jets, and 15.2% for light jets. The integrated luminosity uncertainty is determined to be 6.1%. The uncertainties on the theoretical cross sections of the SM processes are 18% for $t\bar{t}$ production, 9% for $W(Z)+\text{jets}$ production and 6% for WZ/ZZ processes. The uncertainty on the k -factors applied to $W/Z+$ heavy flavor jets processes is assigned to be 20%.

The overall systematic uncertainty obtained by adding the above uncertainties in quadrature are 25% \sim 30% for the background and 16% for the signal.

VIII. LIMIT CALCULATIONS

The cross section limits are derived at 95% Confidence Level (CL) using the so-called “the LEP CL_S method” [20], which is a modified Frequentist CL_S approach with the ratio of two Poisson based binned-likelihood functions (corresponding to *background-only* hypothesis and *signal+background* hypothesis, respectively) as test statistic.

To maximize the search sensitivity, the S_T variable, which efficiently separates the LQ_3 signal from backgrounds, is chosen as the input final discriminant variable for the limit calculation. The systematic uncertainties and the correlations between different background processes and between background and signal are also propagated to the confidence level calculation.

Figure 4 shows the cross section upper limits as functions of the LQ_3 mass, which are derived based on the S_T distributions of the single-tag and double-tags subsamples. Assuming $\beta(LQ_3 \rightarrow \tau b) = 1$, the theoretical prediction of the NLO cross sections of the $p\bar{p} \rightarrow LQ_3\bar{L}Q_3 \rightarrow \tau b\tau b$ at a center-of-mass energy of $\sqrt{s} = 1.96$ TeV is also displayed in Figure 4. The theoretical error band is obtained by adding in quadrature the cross section variations by varying the renormalization and factorization scale from M_{LQ_3} to $0.5M_{LQ_3}$ (upper band) (and to $2M_{LQ_3}$ for lower band), and by PDF uncertainty which is evaluated using the CTEQ prescription [21]. The observed cross section upper limit meets with the theoretical prediction central value at place where LQ_3 mass is 187 GeV, with the lower edge of the cross section error band at place where LQ_3 mass is 180 GeV, and with the upper edge of the cross section error band at place where LQ_3 mass is 195 GeV. The mass of third generation scalar leptoquark is excluded up to 180 GeV at 95% CL, which corresponds to the cross section of the LQ_3 pair production at the Tevatron of 0.42 pb.

Figure 4 also shows the lower edge of the cross section error band for the case when a charge- $\frac{2}{3}$ leptoquark is kinematically allowed to decay to $\nu_\tau t$, supposing that the LQ_3 couplings to the $\nu_\tau t$ and τb are the same, the branching fraction of $LQ_3 \rightarrow b\tau$ is then $1 - 0.5 \times F_{sp}$ where F_{sp} is the phase space suppression factor for the $\nu_\tau t$ channel [7]. This curve is barely displaced with that for $\beta(LQ_3 \rightarrow b\tau) = 1$ within the sensitive region, therefore, the lower leptoquark mass is also set at 180 GeV for this scenario.

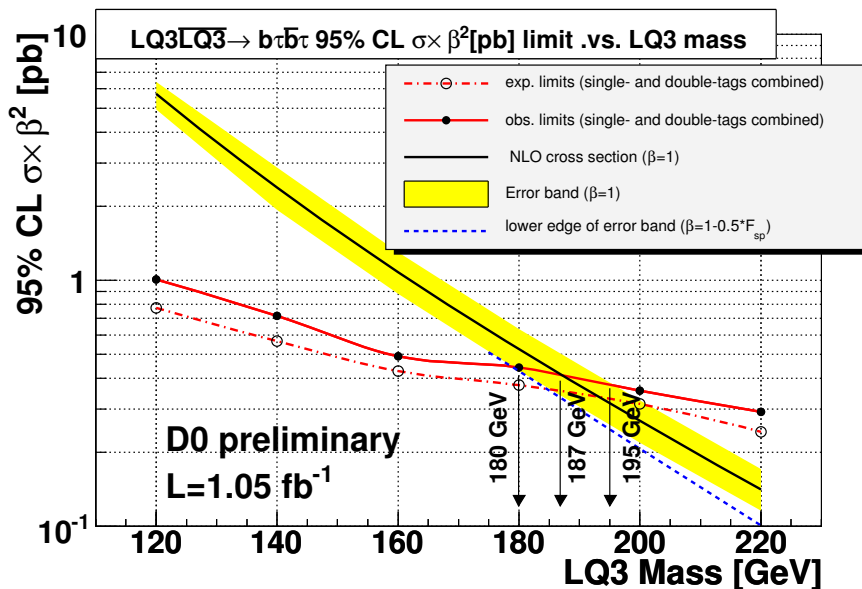


FIG. 4: The observed and expected cross section upper limits of the pair production of third generation leptoquark as the function of the LQ_3 mass. The theoretical prediction is also shown with error bands.

IX. SUMMARY

A search for third generation scalar leptoquark pair production in $p\bar{p}$ collisions at a center-of-mass energy of $\sqrt{s} = 1.96$ TeV has been performed in the $\tau b\tau b$ channel using the data collected by the Run II $D\bar{O}$ detector with an integrated luminosity of 1.05 fb^{-1} . The number of observed data events is consistent with the expectation from Standard Model processes, and no signal evidence has been observed. The limits on the cross sections of third generation leptoquark pair production ($\sigma(p\bar{p} \rightarrow LQ_3 \bar{L}Q_3 \rightarrow \tau b\tau b)$) are set and the mass of the scalar third generation leptoquark predicted by the theory has been excluded at 95% confidence level up to 180 GeV for the case where the LQ_3 decays into a τ lepton and a b quark with a branching fraction $\beta = 1$.

Acknowledgments

We thank the staffs at Fermilab and collaborating institutions, and acknowledge support from the DOE and NSF (USA); CEA and CNRS/IN2P3 (France); FASI, Rosatom and RFBR (Russia); CAPES, CNPq, FAPERJ, FAPESP and FUNDUNESP (Brazil); DAE and DST (India); Colciencias (Colombia); CONACyT (Mexico); KRF and KOSEF (Korea); CONICET and UBACyT (Argentina); FOM (The Netherlands); Science and Technology Facilities Council (United Kingdom); MSMT and GACR (Czech Republic); CRC Program, CFI, NSERC and WestGrid Project (Canada); BMBF and DFG (Germany); SFI (Ireland); The Swedish Research Council (Sweden); CAS and CNSF (China); Alexander von Humboldt Foundation; and the Marie Curie Program.

-
- [1] J.C. Pati and A. Salam, Phys. Rev. D 10 (1974) 275; H. Georgi and S.L. Glashow, Phys. Rev. Lett. 32 (1974) 438.
 - [2] S. Dimopoulos and L. Susskind, Nucl. Phys. B 155 (1979) 237; S. Dimopoulos, Nucl. Phys. B 168 (1980) 69; E. Eichten and K. Lane, Phys. Lett. B 90 (1980) 125.
 - [3] B. Schrempp and F. Schrempp, Phys. Lett. B 153 (1985) 101; W. Buchmüller, R. Rückl and D. Wyler, Phys. Lett. B 191 (1987) 442 [Erratum-ibid. B 448 (1999) 320].
 - [4] F. Abe *et al.* [CDF Collaboration], Phys. Rev. Lett. 78 (1997) 2906.
 - [5] B. Abbott *et al.* [$D\bar{O}$ Collaboration], Phys. Rev. Lett. 81 (1998) 38.
 - [6] T. Affolder *et al.* [CDF Collaboration], Phys. Rev. Lett. 85 (2000) 2056.
 - [7] V. Abazov *et al.* [$D\bar{O}$ Collaboration], arXiv:hep-ex/0705.0812, to be published in Phys. Rev. Lett..
 - [8] The CDF Collaboration, CDF note 8309 (2006).
 - [9] V. Abazov *et al.* [$D\bar{O}$ Collaboration], Nucl. Instrum. and Methods A 463 (2006) 565.
 - [10] T. Sjöstrand *et al.*, Comput. Phys. Commun. 135 (2001) 238; T. Sjöstrand *et al.*, e-Print Archive: hep-ph/0108264 .
 - [11] J. Pumplin *et al.*, J. High Energy Phys. 07 (2002) 12.
 - [12] M. Kramer *et al.*, Phys. Rev. Lett. 79 (1997) 341;
 - [13] M. Mangano *et al.*, e-Print Archive: hep-ph/0206293.
 - [14] S. Höche *et al.*, “ Matching Parton Showers and Matrix Elements”, hep-ph/0602031.
 - [15] S. Jadach *et al.*, Comput. Phys. Commun. 76 (1993) 361.
 - [16] J. Campbell and K. Ellis, “MCFM, Monte-Carlo for $FeMtobarn$ processes”, <http://mcfm.fnal.gov/>.
 - [17] V. Abazov *et al.* [$D\bar{O}$ Collaboration], Phys. Rev. D71 (2005) 072004.
 - [18] V. Abazov *et al.* [$D\bar{O}$ Collaboration], arXiv:hep-ex/0705.2788, to be published in Phys. Rev. D.
 - [19] V. Abazov *et al.* [$D\bar{O}$ Collaboration], Phys. Rev. D75 (2007) 092001.
 - [20] A. Read, J. Phys. G: Nucl. Part. Phys. 28 (2002) 2693; T. Junk, Nucl. Instrum. Methods A 434 (1999) 435.
 - [21] J. Pumplin *et al.*, JHEP 0207, 12(2002); D. Stump *et al.*, JHEP 0310, 046(2003).